ACS APPLIED MATERIALS & INTERFACES

www.acsami.org Research Article

CNTs/LiV_3O_8/Y_2O_3 Composites with Enhanced Electrochemical Performances as Cathode Materials for Rechargeable Solid-State Lithium Metal Batteries

Yuqiang Pi, Zhiwei Gan, Mengyu Yan, Zheng Li, Yushan Ruan, Cunyuan Pei, Hui Yu, Yaowen Ge, Qinyou An,* and Liqiang Mai*

Cite This: *ACS Appl. Mater. Interfaces* 2021, 13, 8219–8228 **Read Online**

ACCESS | Metrics & More | Article Recommendations | Supporting Information

ABSTRACT: Solid-state lithium metal battery (SSLMB) is regarded as a safer energy storage system compared to the liquid one. The performance of the SSLMB depends on the cathode performance and the side reactions derived from the interface of the cathode and the electrolyte, which becomes much severe at high temperatures. Herein, we carried out a facile spray-drying route to prepare a CNTs/LiV_3O_8/Y_2O_3 (M-LVO-Y) composite. The synthesized cathode material exhibits an outstanding Li^+ storage performance with a high reversible capacity of 279.9 mA h g^{-1} at 0.05 A g^{-1}, excellent power capability (182.5 mA h g^{-1} at 2 A g^{-1}), and a long cycle lifespan of 500 cycles with a capacity retention of 66.5% at a current density of 1 A g^{-1}. The fabricated rechargeable solid-state Li/M-LVO-Y-2 lithium metal battery (LMB) with a poly(ethylene oxide) (PEO)-based solid polymer electrolyte (SPE) achieves a high discharge capacity of 302.1 mA h g^{-1} at 0.05 A g^{-1} and a stable cycling performance with the highest capacity of 72.1% after 100 cycles at 0.2 A g^{-1} and 80 °C. The above battery performance demonstrates that SSLMBs with the CNTs/LiV_3O_8/Y_2O_3 cathode and the PEO-based SPE film can provide high energy density and are suitable for applying in a high-temperature environment.

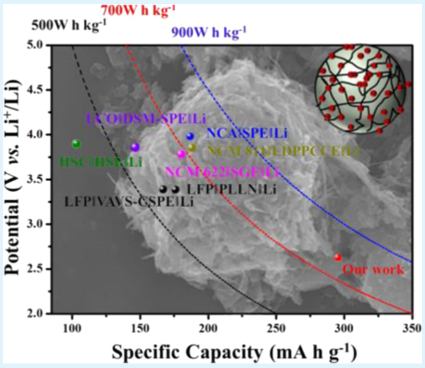

KEYWORDS: *CNTs/LiV_3O_8/Y_2O_3 composite, outstanding Li^+ storage performance, solid-state lithium metal battery, operating temperature, high energy density*

1. INTRODUCTION

Intensive efforts have been put into enhancing the energy density of commercial Li-ion batteries (LIBs) with graphite anodes. Even so, they still cannot satisfy the ever-increasing demands for high energy storage devices.[1−3] Among various anode candidates, the Li metal anode is widely regarded as a potential option, considering its 3860 mA h g^{-1} theoretical capacity and −3.040 V redox potential (vs the standard hydrogen electrode).[4,5] However, there is a noteworthy fact that lithium metal batteries (LMBs) have been considered unsafe systems for a long time, derived from the generation of highly flammable hydrogen gas, the uncontrollable growth of dendritic Li, and the unexpected thermal runaway activity, which hindered the scale applications of LMBs.[6−11] Facing these existing safety challenges, using solid polymer electrolytes (SPEs) instead of the liquid ones has become one of the most effective approaches. SPEs can eliminate the electrolyte flammability and possess sufficient mechanical strength to block the Li dendrites.[12−14] Note that poly(ethylene oxide) (PEO)-based electrolytes are considered the most prospective potential electrolytes among various solid polymer electrolytes (SPEs) because of their prominent Li salt solubility and a low glass transition temperature (T_g).[15,16] Additionally, it is known that temperature is a critical factor for PEO-based SPEs applied in solid-state lithium metal batteries (SSLMBs). Under room temperature, the ionic conductivity of PEO-based SPEs is extremely low, which cannot support sufficient Li-ion migration. When the working temperature is increased, the crystallinity of PEO decreases with the increased ionic conductivity.[17−20] Therefore, it is worth focusing on assembling the PEO-based solid-state batteries for energy storage at high temperatures.

The difference between LMBs and LIBs is mainly derived from the lithium source. Generally, the cathodes of the lithium-ion batteries provide the detachable Li ions. However, upon using the lithium metal as the anode, various non-lithiated cathode materials can be expanded and explored. The layered lithium trivanadate (LiV_3O_8), as one of the non-lithiated cathode materials, has received remarkable attention, owing to

Received: October 22, 2020
Accepted: January 29, 2021
Published: February 9, 2021

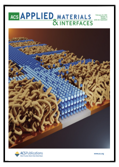

https://dx.doi.org/10.1021/acsami.0c18993

its highlighted specific energy and impressive cycling stability.[21−24] However, the existing issues for LiV_3O_8 commercialization are poor electron transport and structural damage during the processes of Li^+ extraction/insertion, which severely degrade the performance. For solving these issues, a wide variety of strategies have been performed for maintaining the structural integrity and improving the electrical conductivity of LiV_3O_8. For example, the coatings of conductive polymers, graphene oxide, or metal oxides have been proved to be an efficient strategy for improving the Li-ion storage performance of LiV_3O_8.[25−27] The elemental substitution for V is another effective approach accomplished by introducing Mo, Ni, or Si, which can form a mix-valence state of V^{4+}/V^{5+} and provide abundant oxygen vacancies in LiV_3O_8.[28−30] In addition, it has been demonstrated that controlling the morphology of the LiV_3O_8 cathode material has an aggressive impact on its electrochemical performance.[26,31,32]

Y_2O_3, one of the rare earth oxides, has been proved to modify the surface of the electrode material and enhance the electrochemical performance, which is attributed to its splendid thermal stability and good electrical contact with the host material in facilitating electron transfer.[33,34] Furthermore, it is investigated that the crystallinity of PEO is decreased when Y_2O_3 is introduced into PEO-based SPEs, accompanied by the increased electrochemical stability of SPEs.[35] Based on the analyses above, it is of great benefit to dope LiV_3O_8 with Y_2O_3 in PEO-based solid-state lithium metal batteries. Herein, for the first time, we adopted a spray-drying route to synthesize CNTs/LiV_3O_8/Y_2O_3, exhibiting excellent Li-ion storage capability with high discharge capacity, excellent rate performance, and long cycling lifespan. The enhanced electrochemical performance of CNTs/LiV_3O_8/Y_2O_3 is caused by the improvement in electron conductivity and charge transfer kinetics. Furthermore, we designed an all-solid-state LiV_3O_8||PEO-SPE||Li rechargeable lithium metal battery, in which the CNTs/LiV_3O_8/Y_2O_3 composite could achieve a specific capacity of 302.1 mA h g^{-1} at 0.05 A g^{-1} and maintain 72.1% capacity after 100 cycles at 0.2 A g^{-1} and 80 °C. The remarkable electrochemical performance of the SSLMB may be explained by the reduced crystallinity of PEO and the increasing electrochemical stability of the SPE. The successful material and solid-state battery design will facilitate the commercialization of LiV_3O_8 applied as the high-temperature battery cathode.

2. EXPERIMENTAL SECTION

2.1. Preparation of the CNTs/ LiV_3O_8 Composite. A spray-drying and subsequent calcination route was used to prepare the CNTs/LiV_3O_8 composite. In a typical procedure, first, 1.092 kg V_2O_5, 156 g of Li_2CO_3, and 25 mL of $(CH_2OH)_2$ (ethylene glycol) were put into a ball-milling tank with 15 L of CH_3OH (methanol) as the solvent and then continually mixed for 1.5 h. In the subsequent process, the obtained slurry and 700 g of a carbon nanotube conductive paste (5 wt %) were poured into a blender and stirred for 1 h to form a uniform slurry, which then was spray-dried at 205 °C to obtain a solid precursor. Lastly, the mixtures were transferred into a muffle furnace and calcined at 300 °C for 10 h in ambient air, and the obtained products were denoted as M-LVO. The M-LVO sample weighed about 800 g, and more than 200 g of the products were lost, which was mainly ascribed to the fact that the partial intermediate products were stuck to the wall of the spray dryer.

2.2. Preparation of the CNTs/LiV_3O_8/Y_2O_3 Composite. A certain amount of Y_2O_3 and 3 g of M-LVO powders were first poured into isopropyl alcohol and stirred for 1 h. Later, the obtained precursor slurry was dried at 80 °C with stirring continuously. After the solvent was evaporated entirely, the powders obtained were transferred to a vacuum drying oven and kept at 90 °C for 24 h. The samples with ratios of Y_2O_3/M-LVO = 1, 2, 5, and 8% were synthesized and named M-LVO-Y-1, M-LVO-Y-2, M-LVO-Y-5, and M-LVO-Y-8, respectively. The synthetic steps of the CNTs/LiV_3O_8/Y_2O_3 composite are presented in Scheme 1.

Scheme 1. Schematic Diagram of the Synthetic Steps of the CNTs/LiV_3O_8/Y_2O_3 Composite

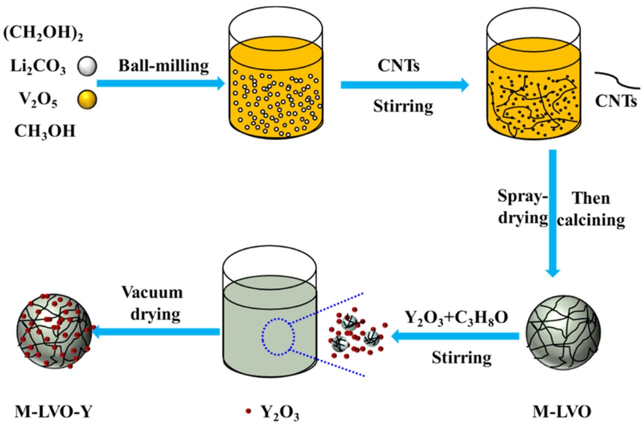

2.3. Preparation of PEO-Based Solid-State Polymer Electrolytes. The PEO-based SPEs were accomplished in a glovebox full of pure argon gas. In a typical preparation, 1.2 g of $LiClO_4$ and 4 g of PEO (EO/Li = 8:1) were first dissolved in 100 g of anhydrous acetonitrile under stirring until a clear solution was afforded. Then, the solution was cast into a homemade Teflon mold and dried at room temperature to form a solid-state polymer electrolyte film, which was cut into round pieces with a diameter of 18 mm for applying in the rechargeable solid-state lithium metal battery

2.4. Material Characterization. The crystallographic information of the final products was collected by performing X-ray diffraction (XRD) measurement on a Bruker D8-Advance X-ray diffractometer with a Cu Kα X-ray source. X-ray photoelectron spectroscopy (XPS) analyses were conducted using an Ultra DLD with a monochromic Al X-ray source. The morphologies of the obtained samples were characterized by a JEOL-7100F microscope. A JEM-2100F microscope was used for recording the images of transmission electron microscopy (TEM).

2.5. Electrochemical Measurement. The electrochemical measurements were conducted with 2016 coin cells assembled in a glovebox full of pure argon gas. In the lithium metal battery (Li metal as the anode), the electrolyte consisted of a 1 M solution of $LiPF_6$ in ethylene carbon (EC)-dimethyl carbonate (DMC) (1:1 w/w), and a polypropylene (PP) film from Celgard served as the separator. The cathode slurry made up of 80 wt % active materials, 10 wt % carbon nanotube conductive paste, and 10 wt % poly(vinylidene difluoride) (PVDF) with a proper amount of an *N*-methyl-2-pyrrolidone (NMP) solvent was coated on an Al foil and dried in a vacuum oven for 24 h at 100 °C. Then, the electrode was cut into 14 mm in diameter circulars with an active material mass loading of 2−2.5 mg cm^{-2}. For the rechargeable solid-state lithium metal battery, the PP films were replaced by PEO-based SPEs, and there was no liquid electrolyte introduced into the battery structure. LAND CT2001A battery test systems were used for carrying out the galvanostatic charge−discharge tests. CHI 760e electrochemical workstations were used for conducting the cyclic voltammetry (CV) and electrochemical impedance spectroscopy (EIS) measurements.

3. RESULTS AND DISCUSSION

The XRD measurements were employed for obtaining the crystallographic information of the final products. It is found from Figure S1 that the diffraction peaks are well indexed to

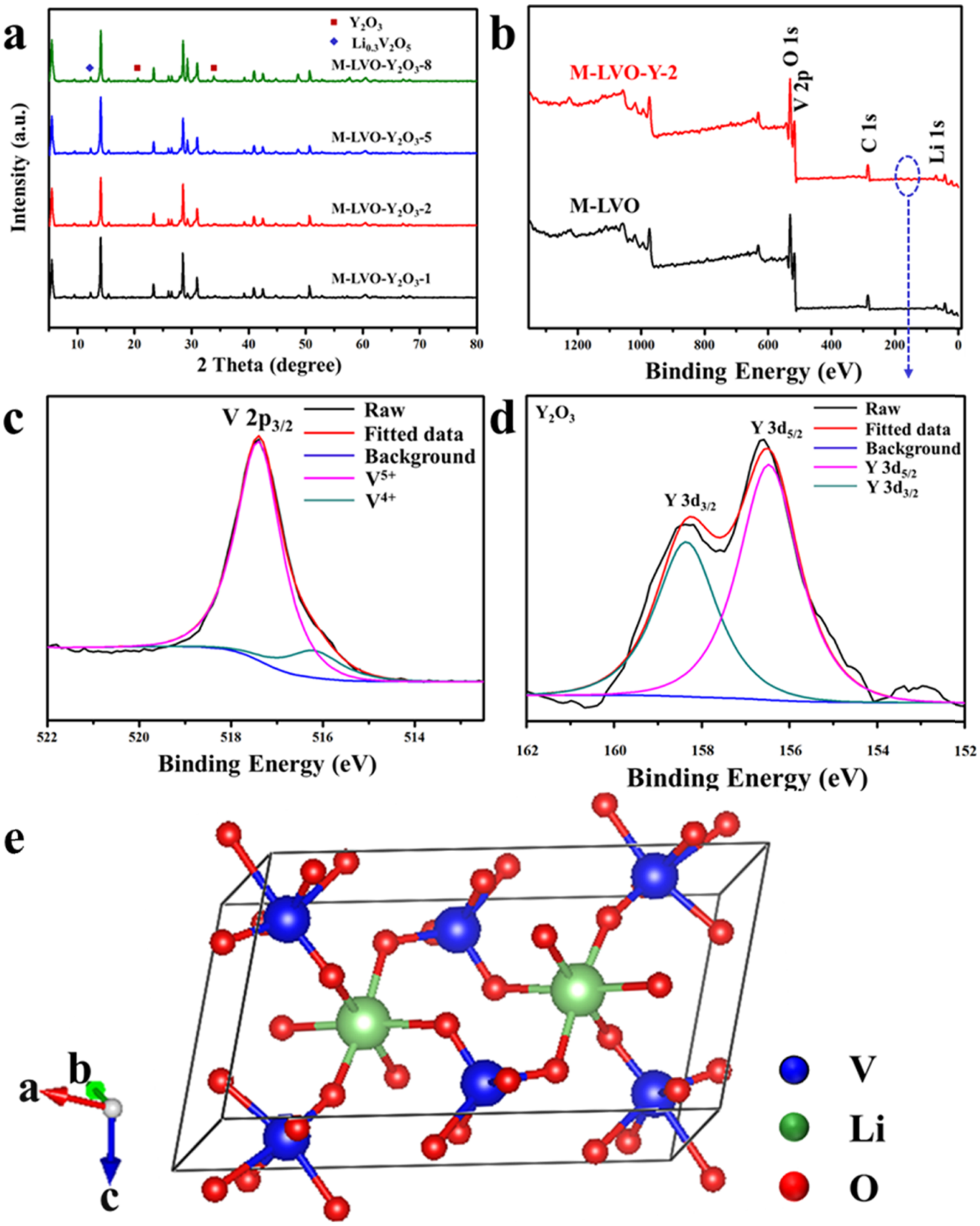

Figure 1. (a) XRD patterns of M-LVO-Y-1, M-LVO-Y-2, M-LVO-Y-5, and M-LVO-Y-8; (b) full XPS spectrum analysis of M-LVO and M-LVO-Y-2; (c) V 2p fine spectrum of M-LVO-Y-2; (d) Y 3d fine spectrum of M-LVO-Y-2; and (e) structure model of the monoclinic LiV_3O_8 and the crystal structure of LiV_3O_8.

layered monoclinic LiV_3O_8 (JCPDS 72-1193, space group: $P2_1/m$), identifying with previous reports.[21,22] As described in Figure 1e, the crystal structure of LiV_3O_8 consisted of V_3O_8 layers interconnecting VO_6 octahedra and VO_5 tetrahedra. Moreover, an impurity phase detected is associated with $Li_{0.3}V_2O_5$, which can be ascribed to the low reaction temperature.[24,36,37] By comparing the XRD patterns of M-LVO-Y (shown in Figure 1a) with those of M-LVO, it is observed that there exist two additional peaks of 20.5 and 33.7°, which are assigned to the phase of Y_2O_3.[38] Furthermore, it could be observed that the intensity of the characteristic peaks of Y_2O_3 is increasing with the increase of Y_2O_3/M-LVO ratios.

XPS measurements were employed for determining the surface composition and element valence. As displayed in Figure 1b, the peaks of O 1s, V 2p, and Li 1s could be clearly observed from the XPS spectra of M-LVO and M-LVO-Y-2. However, on account of the lower Y_2O_3 content in the M-LVO-Y-2 sample, the characteristic peak of Y 3d belonging to Y_2O_3 is not apparent to distinguish it. The peaks ranging from 152 to 162 eV are magnified and recorded in Figure 1d. Two peaks appear at 156.6 and 158.3 eV, which are derived from Y $3d_{5/2}$ and Y $3d_{3/2}$, respectively.[39,40] Based on the XRD and XPS results, it is confirmed that Y_2O_3 is composited with M-LVO. Remarkably, as described in Figure 1c, the V $2p_{3/2}$ XPS spectra presents two peaks at 517.4 and 516.2 eV in the M-LVO-Y-2

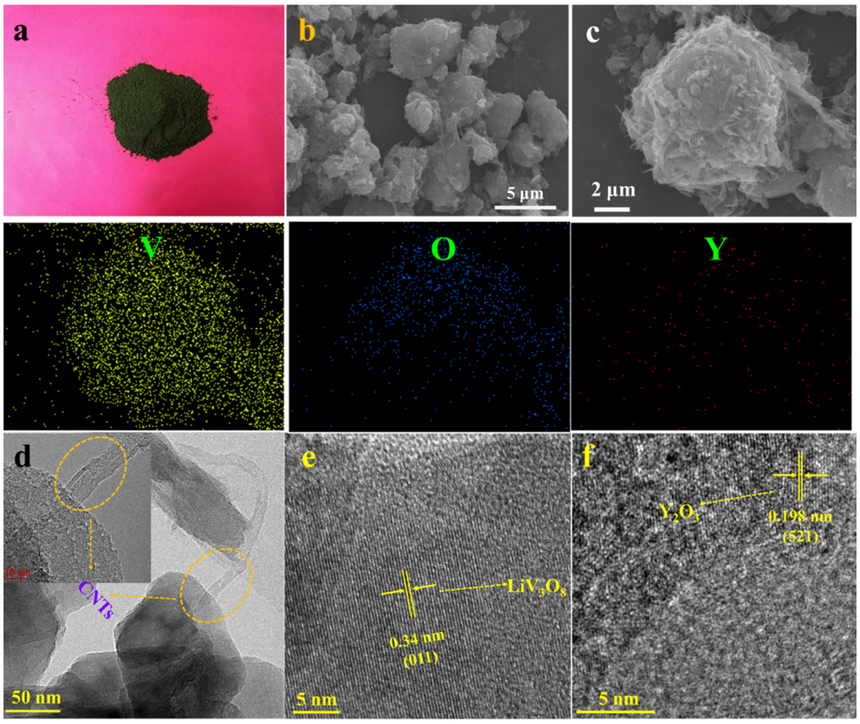

Figure 2. (a) Electronic image of the final products; (b, c) SEM images of M-LVO-Y-2; accompanying diagram of (c) is the corresponding EDS elemental mapping; and (d−f) TEM and HRTEM images of M-LVO-Y-2.

sample. The peak at 517.4 eV is identified as pentavalent vanadium (V^{5+}), and tetravalent vanadium is found at the peak of 516.2 eV, suggesting the mixed V^{4+}/V^{5+} state. It is well known that V^{4+}/V^{5+} coexisting in LiV_3O_8 means the existence of oxygen vacancies and the changes in the structure, which facilitate the formation of percolated pathways for electron hopping between V^{5+} and V^{4+}, accompanied by the improvement in electrical conductivity.[41] By calculating the ratio of the peak areas, it can be concluded that the V^{5+}-to-V^{4+} ratio is calculated about 6.64:1. In fact, the presence of tetravalent V can be expected, derived from the reduction of CNTs and the inert annealing atmosphere.[31]

The electronic image of the final products is displayed in Figure 2a. It is observed that the color of the M-LVO-Y-2 sample is dark green. The morphologies of M-LVO and M-LVO-Y-2 are studied by using the measurement of SEM. As observed in Figures 2b,c, and S2, bulk morphologies accompanied by the partial microspheres are successfully gained via the spray-drying method. Moreover, the elements of V, O, and Y are distributed uniformly in the M-LVO-Y-2 composite. Due to the lack of introduced Y_2O_3, there is no Y element observed in the M-LVO sample. TEM measurement is performed to verify the existence of CNTs, which is expected to improve the electronic conductivity. As shown in Figures 2d and S2b, it is evident that the host material of LiV_3O_8 is covered and embedded by the CNTs. The lattice fringes with the *d*-spacings of 0.34 and 0.575 nm can be clearly observed in Figures 2e and S2b, corresponding to the (011) and (002) planes of LiV_3O_8, respectively. Moreover, Figure 2f presents the lattice fringe with a *d*-spacing of 0.198 nm, recognized as the (521) plane of Y_2O_3, which verifies further synthesis of the $CNTs/LiV_3O_8/Y_2O_3$ composite.

Figure 3 presents the comparison of Li-ion storage capability in the liquid Li metal battery between M-LVO and M-LVO-Y in a potential range of 2.0−3.65 V. CV measurements were conducted at a scan rate of 0.1 mV s^{-1}. The second-cycle CV curves of M-LVO and M-LVO-Y-2 are presented in Figure 3a. Apparently, the M-LVO-Y-2 electrode possesses a larger curve area and higher redox peak current than those of M-LVO, which indicates the higher capacity and the faster kinetics of the M-LVO-Y-2 electrode for Li-ion insertion/extraction.[24,42,43] For the M-LVO and M-LVO-Y-2 electrodes, there exist three pairs of redox peaks at 2.85/2.79, 2.71/2.51, and 2.47/2.31V, respectively, which correspond to the electrochemical behavior of LiV_3O_8 with a reversible process of Li^+ extraction/insertion ($LiV_3O_8 + 3\ Li^+ + 3e^- \leftrightarrow Li_4V_3O_8$).[24,44] In addition, the peak at around 2.87 V for the oxidation process and the pair of anodic/cathodic peaks at 3.45 and 3.42 V have been proved from $Li_{0.3}V_2O_5$ detected from the XRD patterns.[24,27] However, it is noteworthy that there is no increase or decrease in the potential difference between any pair of redox peaks of the M-LVO and M-LVO-Y-2 electrodes because of Y_2O_3 introduced into M-LVO. The phenomenon can be confirmed further by calculating the capacity retention of long cycles. To get insights into the difference of Li-ion storage performance between the M-LVO and M-LVO-Y electrodes, the rate performance evaluated at step current densities varying from 0.05 to 2 A g^{-1} is recorded in Figure 3b. It is evident that the M-LVO-Y-2 electrode shows superior rate capability and delivers higher reversible capacities of 279.9, 257.6, 242.8, 223, 204.1, and 182.5 mA h g^{-1} at current densities of 0.05, 0.1, 0.2, 0.5, 1, and 2 A g^{-1}, respectively. When the current density returns back to 0.05 A g^{-1}, a discharge specific capacity as high as 254.9 mA h g^{-1} can be achieved with a 91.1% capacity retention. The expected rate capability is definitely caused by the enhanced electron conductivity, arising from the nature of the high electrical conductivity of CNTs[45−48] and the percolated pathways for electron hopping between V^{5+} and V^{4+}. Moreover, the M-LVO-Y-2 electrode shows superior rate capability compared to

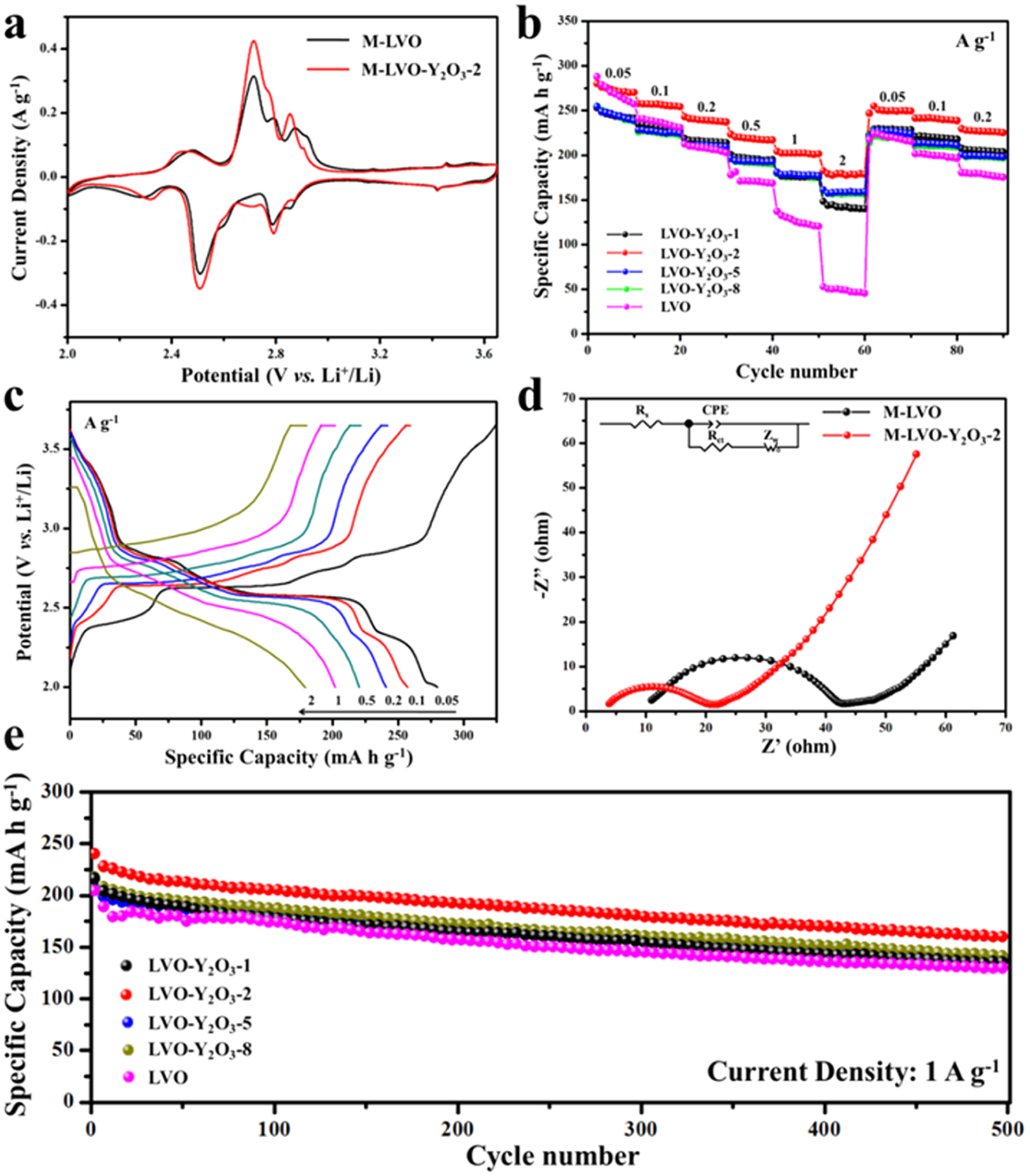

Figure 3. Li-ion storage capability of M-LVO and M-LVO-Y in the liquid Li metal battery in a potential range of 2.0−3.65 V; (a) CV curves of the M-LVO and M-LVO-Y-2 electrodes at a scan rate of 0.1 mV s^{-1}; (b) rate capability of the M-LVO and M-LVO-Y electrodes; (c) galvanostatic charge and discharge curves of M-LVO-Y-2 at varied current densities from 0.05 to 2 A g^{-1}; (d) the Nyquist plots of the M-LVO and M-LVO-Y-2 electrodes after 500 cycles at 1 A g^{-1} with the equivalent circuit inset; and (e) cycling performances of the M-LVO and M-LVO-Y electrodes at 1 A g^{-1}.

M-LVO-Y-1, M-LVO-Y-5, and M-LVO-Y-8. This may be ascribed to 2 wt % Y_2O_3 coating as the most effective coating amount. As the coating amount increased, the active site of LVO decreased, accompanied by the decreased discharge capacity.

Figure 3c displays the galvanostatic charge and discharge curves of M-LVO-Y-2 at varied current densities from 0.05 to 2 A g^{-1}. Remarkably, the result of the three main pairs of charging and discharging platforms appearing in the curves at lower current density is in keeping with the result of CV curves. Moreover, the long cycling stabilities of the M-LVO and M-LVO-Y electrodes are evaluated at a high current density of 1 A g^{-1} for 500 cycles. As shown in Figure 3e, the highest initial discharge specific capacity of 240.2 mA h g^{-1} can be achieved for the M-LVO-Y-2 electrode. After 500 cycles, the M-LVO-Y-2 electrode can maintain 66.5% of the initial capacity, reaching 159.7 mA h g^{-1}, indicating that M-LVO-Y-2 can show remarkable long cycling stability at high current density. Interestingly, for comparison, M-LVO, M-LVO-Y-1, M-LVO-Y-5, and M-LVO-Y-8 can provide the initial discharge specific capacities of 204.4, 216.6, 210.3, and 218 mA h g^{-1} with the capacity retentions of 63.2, 62.7, 67.3, and 64.8% after 500 cycles, respectively. Therefore, a proof by fact is that the content of Y_2O_3 combined with M-LVO can affect the initial discharge specific capacity of the composite but exert a weak influence on capacity retention.

Then, we carried out the EIS measurement for the lithium metal battery after testing the long-term cyclability of M-LVO and M-LVO-Y-2. It is well known that the value of R_{ct} represents the charge transfer resistance. As described in

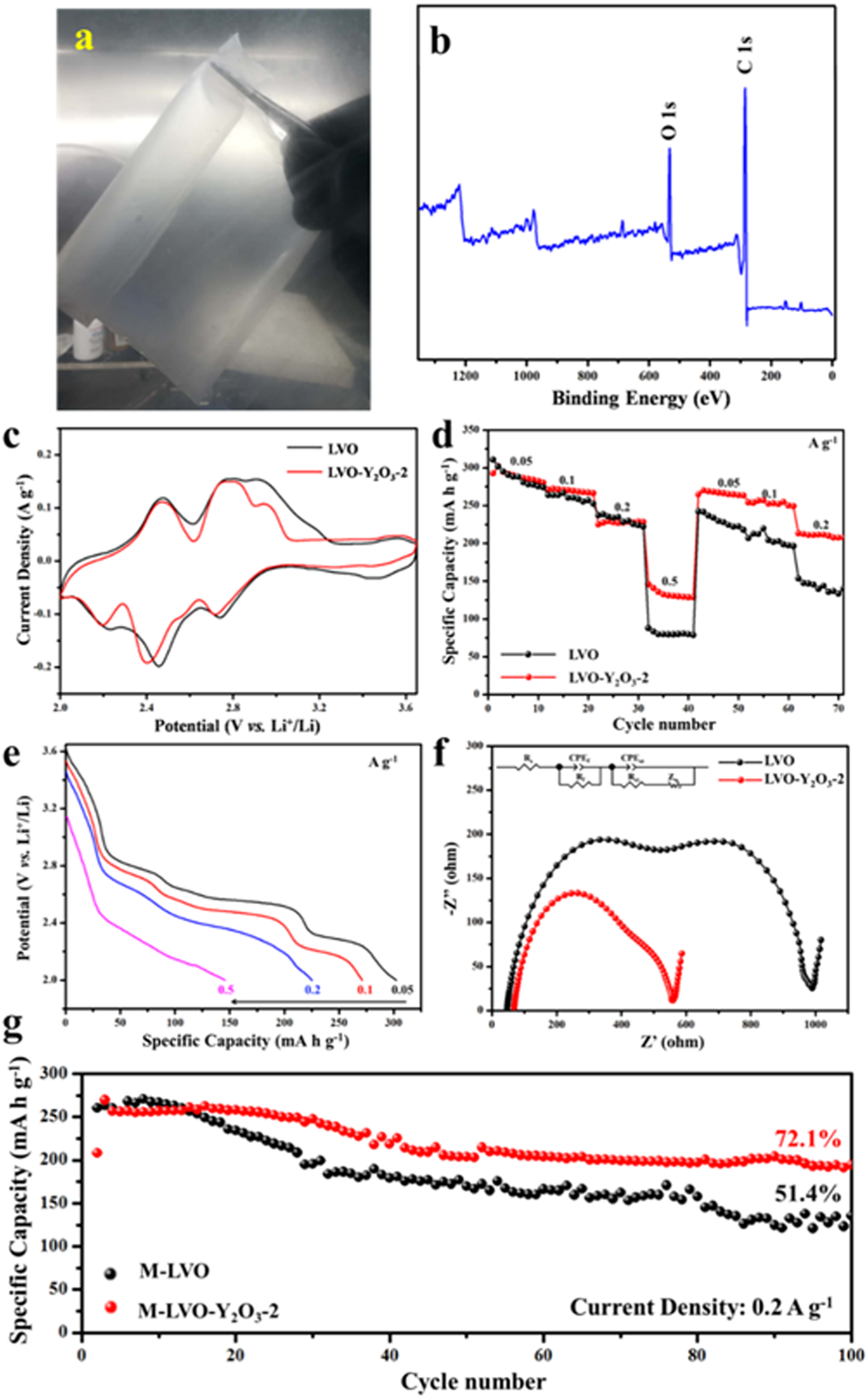

Figure 4. (a) Electronic image of the PEO-based SPE film; (b) full XPS spectrum of the PEO-based SPE film; (c) CV curves of the M-LVO and M-LVO-Y-2 electrodes at a scan rate of 0.1 mV s^{-1} in a potential range of 2.0−3.65 V versus Li/Li$^+$ under an operating temperature of 80 °C in the PEO-based SSLMB; (d) rate performance of the M-LVO and M-LVO-Y-2 electrodes; (e) galvanostatic charge and discharge curves of M-LVO-Y-2 at varied current densities from 0.05 to 0.5 A g^{-1}; (f) the Nyquist plots of the M-LVO and M-LVO-Y-2 electrodes after the rate performance tested with the equivalent circuit inset; and (g) cycling performance of the M-LVO and M-LVO-Y-2 electrodes at 0.2 A g^{-1}.

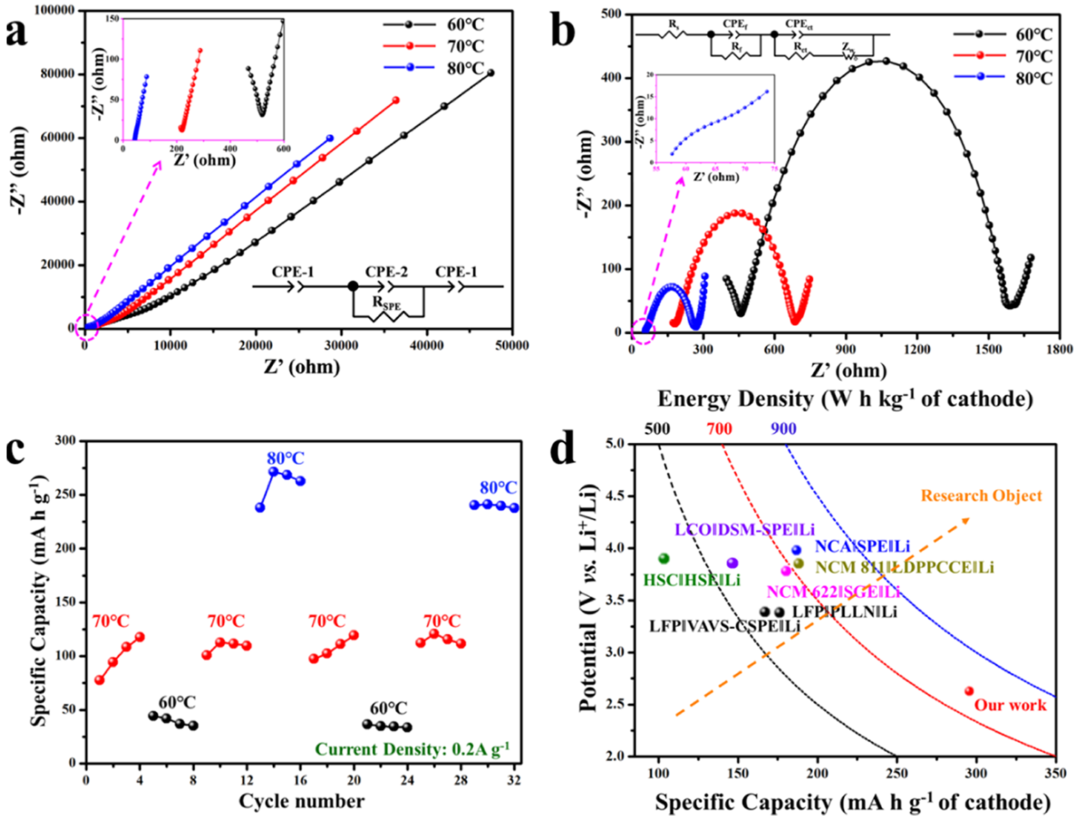

Figure 5. (a, b) Nyquist plots of the PEO-based solid-state polymer film and the LVO/PEO-based solid-state lithium metal battery with the equivalent circuit inset at varied temperatures from 60 to 80 °C, respectively; (c) the correlation between the discharge capacity and the operating temperature for M-LVO-Y-2 electrodes at a current density of 0.2 A g^{-1}; (d) comparison of the energy density of the LVO/PEO-based solid-state lithium metal battery with recent results reported in the literature for solid-state Li metal batteries (LFP||VAVS-CSPE||Li,[12] LFP||PLLN||Li,[49] HSC||HSE||Li,[50] NCM 622||SGE||Li,[51] NCM 811||LDPPCCE||Li,[52] NCA||SPE||Li,[53] and LCO||DSM-SPE||Li[14]).

Figure 3d, an R_{ct} of 21.2 Ω for the M-LVO-Y-2 electrode is much smaller than that of M-LVO (42.4 Ω), suggesting that introduction of Y_2O_3 into the LiV_3O_8 host material can improve the charge transfer kinetics.

Additionally, we compared the cycling performance of the M-LVO-Y-2 electrode in the liquid LMB at room temperature and at a high temperature of 80 °C. As shown in Figure S3, as the M-LVO-Y-2 electrode is charged and discharged at a current density of 0.2 A g^{-1}, the initial discharge specific capacity of 294.3 mA h g^{-1} at 80 °C is much higher than that of 242.3 mA h g^{-1} at room temperature, which may be ascribed to the destructive decomposition to the liquid organic electrolyte at a high temperature. With the increasing cycles, the discharge capacity at 80 °C presents a trend of sharp decline and only achieves 104.4 mA h g^{-1} after 110 cycles, indicating a 35.5% capacity retention. However, the M-LVO-Y-2 electrode after 250 cycles at room temperature still maintains 77.8% of the initial capacity, reaching 188.4 mA h g^{-1}. Therefore, from the perspective of capacity retention, it is compelled to admit that the rechargeable Li metal battery with the liquid organic electrolyte is hard to be promoted in a harsh environment at a high temperature. It is necessary to design a special high-temperature battery, and the SSLMB should be one of the various viable options.

3.1. CNTs/LiV3O8/Y2O3 Cathode Materials for the Rechargeable SSLMB. The electronic image of the PEO-based SPE film is displayed in Figure 4a. It clearly shows the transparency and flexibility of the SPE film. XPS measurements were employed to verify the composition of the PEO-based SPE film. As shown in Figure 4b, two apparent peaks appear in the XPS spectrum, assigned to O 1s and C 1s, mainly originating from the PEO polymer. Moreover, after the M-LVO-Y composite was applied in the liquid lithium metal battery successfully, it is of great necessity to demonstrate its practical feasibility for the rechargeable SSLMB.

Figure 4c presents the CV curves of the M-LVO and M-LVO-Y-2 electrodes applied in the PEO-based SSLMB in a potential range of 2.0−3.65 V at 80 °C. Apparently, three pairs of main redox peaks can be found in the liquid LMB appearing at 2.94/2.73, 2.79/2.43, and 2.46/2.19 V in the M-LVO-Y-2 composite, respectively. This can be ascribed to the phase transitions from LiV_3O_8 to $Li_4V_3O_8$. The redox peaks at 3.55/3.45 V derived from the existence of impurity phase $Li_{0.3}V_2O_5$ can still be detected. Figure 4d is the rate performance comparison of two obtained samples at step current densities varied from 0.05 to 0.5 A g^{-1}. For the M-LVO-Y-2 electrode, the superior rate capability can be possessed with reversible capacities of 302.1, 271, 225.1, and 145.6 mA h g^{-1} at current densities of 0.05, 0.1, 0.2, and 0.5 A g^{-1}, respectively. While the current density reverses to 0.05 A g^{-1}, it could still achieve a high capacity of 270 mA h g^{-1} with an 89.4% capacity retention. The same test procedure was carried out for the M-LVO-Y electrodes, which can only maintain 77.7% of the initial capacity as high as 310.7 mA h g^{-1} after 30 cycles. In addition, according to the galvanostatic charge and discharge curves of M-LVO-Y-2 shown in Figure 4e, there are three platforms observed in the curves, identified with the result of the CV measurement.

https://dx.doi.org/10.1021/acsami.0c18993
ACS Appl. Mater. Interfaces 2021, 13, 8219−8228

After testing the rate performance of two kinds of electrodes, the EIS spectrum is recorded in Figure 4f with the equivalent circuit inset, which is made up of two semicircles in high- and medium-frequency regions and a straight sloping line in the low-frequency regions. As described in the equivalent circuit, R_s corresponds to the internal resistance of the battery, containing the particle−particle resistance, the electrolyte resistance, and the resistance derived from the electrodes and the current collectors, and R_f and R_{ct} refer to the resistance of the solid electrolyte interface (SEI) film and the charge transfer resistance, respectively.[49,50] It is evident that the R_{ct} of M-LVO-Y-2 is much smaller than that of M-LVO, which may be ascribed to the dual functions of Y_2O_3 by improving the charge transfer kinetics of the LiV_3O_8 host material and reducing the crystallinity of PEO, accompanied by the increasing electrochemical stability of SPE.[35]

Moreover, the cycling lifespans of M-LVO and M-LVO-Y-2 are studied at a current density of 0.2 A g^{-1} (Figure 4g). The trend of discharging capacities from increasing to decreasing may be caused by the electrochemical activation of the electrodes and the SPE film. Within the cycling, the highest capacities of the M-LVO and M-LVO-Y-2 electrodes are 263.6 and 269.6 mA h g^{-1}, respectively. M-LVO-Y-2 possesses a capacity of 194.5 mA h g^{-1}, indicating 72.1% of the highest capacity after 100 cycles. In contrast, the two values above associated with M-LVO are 51.4% and 135.6 mA h g^{-1}. It is noteworthy that the electrochemical performance of M-LVO-Y-2 with extremely high electrode piece quality is also presented in Figure S4. Compared with the low loading of the electrode, a similar discharging capacity trend can be also gained. Moreover, as shown in Figure S4b, it is evident that the curves of M-LVO-Y-2 with extremely high electrode piece quality are similar to those with low loading, as described in Figure 4e. As above, concerning the capacity retention of the M-LVO-Y-2 electrode at 80 °C, we compared the SSLMB with the liquid LMB as a consequence and found that the LVO/PEO-based SSLMB is more suitable for applying in a harsh environment at a high temperature.

To investigate the relationship between the PEO-based solid-state polymer film and the operating temperature, CR2016 coin cells consisting of the Li metal anode, the PEO-based SPE film, and the block electrode were adopted with the current collector. As shown in Figure 5a, there is an interesting result coming from the EIS spectrum of the PEO-based SPE film from 60 to 80 °C. The value of R_{SPE} related to the electrolyte resistance of the PEO-based solid-state polymer film and the interface resistance declines as the temperature increases from 60 to 80 °C. In addition, the open-circuit potentials (OCP) of the PEO-based SPE film at different operating temperatures of 60, 70, and 80 °C are recorded and assigned to 2.465, 2.509, and 2.577 V, respectively. Moreover, EIS measurements were also performed for M-LVO-Y-2 electrodes to explore the correlation of R_{ct} (charge transfer resistance) with different operating temperatures. Figure 5b demonstrates that the value of R_{ct} presents a decreasing trend with the increasing operating temperature, indicating that R_{ct} is negatively correlated with the operating temperature.

As is known to all, the Arrhenius equation, $k = A\,e^{-E_a/RT}$ or $\ln k = -E_a/RT + \ln A$, can be used to explore how the rate of a reaction depends on temperature.[51] In this equation, K, R, A, T, and E_a are the rate constant, gas constant, frequency factor, absolute temperature, and activation energy, respectively. In the case of the PEO-based SPE, it can be found that E_a increase with the increase of absolute temperature, accompanied by the increase of the conductivity of the PEO-based SPE. Remarkably, it can be concluded that R_{SPE} is negatively correlated with the operating temperature. Moreover, as is known to all, OCP is directly related to R_{SPE}. As R_{SPE} decreases, the value of OCP increases. Therefore, a conclusion can be obtained that OCP is negatively correlated with R_{SPE} under different operating temperatures. Similarly, R_{ct} is negatively correlated with the operating temperature.

Furthermore, the correlation between the discharge capacity and the operating temperature for the M-LVO-Y-2 electrode is recorded in Figure 5c. Apparently, it displays the highest capacity of 271.3 mA h g^{-1} under 80 °C at a current density of 0.2 A g^{-1}, while only 44.4 mA h g^{-1} can be achieved under 60 °C. The gap of the discharge capacities under different operating temperatures can be distinguished visibly. Moreover, a comparison of the energy density of the SSLMB reported in the literature is shown in Figure 5.[14,16,52−56] To the best of our knowledge, the key factor of developing high energy storage devices is the cathode. Although the M-LVO-Y-2 electrode applied in the SSLMB possesses a lower average discharge voltage of 2.58 V, it can deliver the highest specific capacity than cathodes in the application reported above. Therefore, for the M-LVO-Y-2 electrode, the energy density estimated to be 779.4 W h kg^{-1} is also far higher than other cathodes. All in all, the $CNTs/LiV_3O_8/Y_2O_3$ composite exhibiting excellent electrochemical performance may be a successful option for a practical solid-state lithium metal battery applied in a harsh environment at a high temperature.

4. CONCLUSIONS

$CNTs/LiV_3O_8/Y_2O_3$ composite was prepared successfully by a simple spray-drying route. As a potential cathode material applied in the LMB, the $CNTs/LiV_3O_8$ composite introduced with 2 wt % Y_2O_3 exhibits outstanding Li-ion storage capability with a high reversible capacity of 279.9 mA h g^{-1} at 0.05 A g^{-1}, superior power capability (182.5 mA h g^{-1} at 2 A g^{-1}), and a long cycle lifespan of 500 cycles with a 66.5% capacity retention at a current density of 1 A g^{-1}. The impressive performance is caused by the introduced CNTs and Y_2O_3 for improving the electron conductivity of the LiV_3O_8 host material and the charge transfer kinetics. Moreover, the rechargeable solid-state Li/M-LVO-Y-2 lithium metal battery with the PEO-based SPE film shows a higher capacity of 302.1 mA h g^{-1} at 0.05 A g^{-1} and gives a stable cycling performance with 72.1% of the highest capacity after 100 cycles at 0.2 A g^{-1} under 80 °C, and Y_2O_3 can play a significant role in reducing the crystallinity of PEO. In addition, by conducting EIS measurements and capacity characterization at different operating temperatures, the result demonstrates the strong impact of the operating temperature exerted on the open-circuit potentials (OCP) of the PEO-based SPE film and the charge transfer resistance of the PEO-based SSLMB. Significantly, it is proved that solid-state lithium metal batteries containing the $CNTs/LiV_3O_8/Y_2O_3$ cathode and the PEO-based SPE film can provide extremely higher energy density and are suitable for applying in a harsh environment at a high temperature.

■ ASSOCIATED CONTENT

Supporting Information

The Supporting Information is available free of charge at https://pubs.acs.org/doi/10.1021/acsami.0c18993.

XRD patterns of M-LVO; SEM, TEM, and HRTEM images of M-LVO; cycling performance of M-LVO-Y-2 electrodes in the liquid Li metal battery between room temperature and 80 °C at a current density of 0.2 A g^{-1}; electrochemical performance of M-LVO-Y-2 with extremely high piece quality (PDF)

AUTHOR INFORMATION

Corresponding Authors

Qinyou An − *State Key Laboratory of Advanced Technology for Materials Synthesis and Processing, Wuhan University of Technology, Hubei, Wuhan 430070, China; Foshan Xianhu Laboratory of the Advanced Energy Science and Technology Guangdong Laboratory, Guangdong, Foshan 528200, China;* orcid.org/0000-0003-0605-4942; Email: mlq518@whut.edu.cn

Liqiang Mai − *State Key Laboratory of Advanced Technology for Materials Synthesis and Processing, Wuhan University of Technology, Hubei, Wuhan 430070, China; Foshan Xianhu Laboratory of the Advanced Energy Science and Technology Guangdong Laboratory, Guangdong, Foshan 528200, China;* orcid.org/0000-0003-4259-7725; Email: anqinyou86@whut.edu.cn

Authors

Yuqiang Pi − *State Key Laboratory of Advanced Technology for Materials Synthesis and Processing, Wuhan University of Technology, Hubei, Wuhan 430070, China*

Zhiwei Gan − *State Key Laboratory of Advanced Technology for Materials Synthesis and Processing, Wuhan University of Technology, Hubei, Wuhan 430070, China*

Mengyu Yan − *State Key Laboratory of Advanced Technology for Materials Synthesis and Processing, Wuhan University of Technology, Hubei, Wuhan 430070, China*

Zheng Li − *WUT Powerful Energy Co., Ltd., Hubei, Wuhan 430223, China*

Yushan Ruan − *State Key Laboratory of Advanced Technology for Materials Synthesis and Processing, Wuhan University of Technology, Hubei, Wuhan 430070, China*

Cunyuan Pei − *State Key Laboratory of Advanced Technology for Materials Synthesis and Processing, Wuhan University of Technology, Hubei, Wuhan 430070, China*

Hui Yu − *State Key Laboratory of Advanced Technology for Materials Synthesis and Processing, Wuhan University of Technology, Hubei, Wuhan 430070, China*

Yaowen Ge − *WUT Powerful Energy Co., Ltd., Hubei, Wuhan 430223, China*

Complete contact information is available at: https://pubs.acs.org/10.1021/acsami.0c18993

Notes

The authors declare no competing financial interest.

ACKNOWLEDGMENTS

This work was supported by the National Key Research and Development Program of China (2020YFA0715000,2017YFE0127600, 2016YFA0202600), the National Natural Science Foundation of China (51972259), and the Hubei Provincial Natural Science Foundation of China (2019CFB519).

REFERENCES

(1) Goodenough, J. B.; Kim, Y. Challenges for Rechargeable Li Batteries. *Chem. Mater.* **2010**, *22*, 587−603.

(2) Armand, M.; Tarascon, J. M. Building Better Batteries. *Nature* **2008**, *451*, 652−657.

(3) Tarascon, J. M.; Armand, M. Issues and Challenges Facing Rechargeable Lithium Batteries. *Nature* **2001**, *414*, 359−367.

(4) Lin, D.; Liu, Y.; Cui, Y. Reviving the Lithium Metal Anode for High-Energy Batteries. *Nat. Nanotechnol.* **2017**, *12*, 194−206.

(5) Xu, W.; Wang, J.; Ding, F.; Chen, X.; Nasybutin, E.; Zhang, Y.; Zhang, J. Lithium Metal Anodes for Rechargeable Batteries. *Energy Environ. Sci.* **2014**, *7*, 513−537.

(6) Li, N.; Shi, Y.; Yin, Y.; Zeng, X.; Li, J.; Li, C.; Wan, L.; Wen, R.; Guo, Y. A Flexible Solid Electrolyte Interphase Layer for Long-Life Lithium Metal Anodes. *Angew. Chem., Int. Ed.* **2018**, *57*, 1505−1509.

(7) Chen, M.; Liu, J.; Ouyang, D.; Cao, S.; Wang, Z.; Wang, J. A Simplified Analysis to Predict the Fire Hazard of Primary Lithium Battery. *Appl. Sci.* **2018**, *8*, No. 2329.

(8) Lisbona, D.; Snee, T. A Review of Hazards Associated with Primary Lithium and Lithium-Ion Batteries. *Process Saf. Environ. Prot.* **2011**, *89*, 434−442.

(9) Liu, B.; Zhang, J.; Xu, W. Advancing Lithium Metal Batteries. *Joule* **2018**, *2*, 833−845.

(10) Liu, G.; Weng, W.; Zhang, Z.; Wu, L.; Yang, J.; Yao, X. Densified Li_6PS_5Cl Nanorods with High Ionic Conductivity and Improved Critical Current Density for All-Solid-State Lithium Batteries. *Nano Lett.* **2020**, *20*, 6660−6665.

(11) Wan, H.; Cai, L.; Han, F.; Mwizerwa, J. P.; Wang, C.; Yao, X. Construction of 3D Electronic/Ionic Conduction Networks for All-Solid-State Lithium Batteries. *Small* **2019**, *15*, No. 1905849.

(12) Zhou, W.; Wang, S.; Li, Y.; Xin, S.; Manthiram, A.; Goodenough, J. B. Plating aDendrite-Free Lithium Anode with a Polymer/Ceramic/Polymer Sandwich Electrolyte. *J. Am. Chem. Soc.* **2016**, *138*, 9385−9388.

(13) Bouchet, R.; Maria, S.; Meziane, R.; Aboulaich, A.; Lienafa, L.; Bonnet, J. P.; Phan, T. N. T.; Bertin, D.; Gigmes, D.; Devaux, D.; Denoyel, R.; Armand, M. Single-ion BAB Triblock Copolymers as Highly Efficient Electrolytes for Lithium-Metal Batteries. *Nat. Mater.* **2013**, *12*, 452−457.

(14) Tang, W.; Tang, S.; Guan, X.; Zhang, X.; Xiang, Q.; Luo, J. High-Performance Solid Polymer Electrolytes Filled with Vertically Aligned 2D Materials. *Adv. Funct. Mater.* **2019**, *29*, No. 1900648.

(15) Yang, C.; Fu, K.; Zhang, Y.; Hitz, E.; Hu, L. Protected Lithium-Metal Anodes in Batteries: From Liquid to Solid. *Adv. Mater.* **2017**, *29*, No. 1701169.

(16) Wang, C.; Wang, T.; Wang, L.; Hu, Z.; Cui, Z.; Li, J.; Dong, S.; Zhou, X.; Cui, G. Differentiated Lithium Salt Design for Multilayered PEO Electrolyte Enables a High-Voltage Solid-State Lithium Metal Battery. *Adv. Sci.* **2019**, *6*, No. 1901036.

(17) Choudhary, S.; Sengwa, R. J. Effects of Different Inorganic Nanoparticles on the Structural, Dielectric and Ion Transportation Properties of Polymers Blend Based Nanocomposite Solid Polymer Electrolytes. *Electrochim. Acta* **2017**, *247*, 924−941.

(18) Ben Youcef, H.; Garcia-Calvo, O.; Lago, N.; Devaraj, S.; Armand, M. Cross-Linked Solid Polymer Electrolyte for All-Solid-State Rechargeable Lithium Batteries. *Electrochim. Acta* **2016**, *220*, 587−594.

(19) Scrosati, B.; Garche, J. Lithium Batteries: Status, Prospects and Future. *J. Power Sources* **2010**, *195*, 2419−2430.

(20) Moreno, M.; Quijada, R.; Santa Ana, M. A.; Benavente, E.; Gomez-Romero, P.; Gonzalez, G. Electrical and Mechanical Properties of Poly(ethylene oxide)/Intercalated Clay Polymer Electrolyte. *Electrochim. Acta* **2011**, *58*, 112−118.

(21) Chen, Z.; Xu, F.; Cao, S.; Li, Z.; Yang, H.; Ai, X.; Cao, Y. High Rate, Long Lifespan LiV_3O_8 Nanorods as a Cathode Material for Lithium-Ion Batteries. *Small* **2017**, *13*, No. 1603148.

(22) Ren, W.; Zheng, Z.; Luo, Y.; Chen, W.; Niu, C.; Zhao, K.; Yan, M.; Zhang, L.; Meng, J.; Mai, L. An Electrospun Hierarchical LiV_3O_8

Nanowire-In-Network for High-Rate and Long-Life Lithium Batteries. *J. Mater. Chem. A* **2015**, *3*, 19850−19856.

(23) Mei, P.; Wu, X.; Xie, H.; Sun, L.; Zeng, Y.; Zhang, J.; Tai, L.; Guo, X.; Cong, L.; Ma, S.; Yao, C.; Wang, R. LiV_3O_8 Nanorods as Cathode Materials for High-Power and Long-Life Rechargeable Lithium-Ion Batteries. *RSC Adv.* **2014**, *4*, 25494−25501.

(24) Xu, X.; Luo, Y.; Mai, L.; Zhao, Y.; An, Q.; Xu, L.; Hu, F.; Zhang, L.; Zhang, Q. Topotactically Synthesized Ultralong LiV_3O_8 Nanowire Cathode Materials for High-Rate and Long-Life Rechargeable Lithium Batteries. *NPG Asia Mater.* **2012**, *4*, e20.

(25) Bae, K. Y.; Park, G. D.; Kim, B. H.; Cho, S. H.; Kang, Y. C.; Lee, K. D.; Yoon, W. Y. Improving the Electrochemical Performance of Lithium Metal Batteries with Hollow Shell Microspheres and Polypyrrole Vapor Phase-Coated LiV_3O_8 Cathodes. *J. Electrochem. Soc.* **2018**, *165*, A2919−A2924.

(26) Mo, R.; Du, Y.; Rooney, D.; Ding, G.; Sun, K. Ultradispersed Nanoarchitecture of LiV_3O_8 Nanoparticle/Reduced Graphene Oxide with High Capacity and Long-Life Lithium-Ion Battery Cathodes. *Sci. Rep.* **2016**, *6*, No. 19843.

(27) Huang, S.; Tu, J.; Jian, X.; Lu, Y.; Shi, S.; Zhao, X.; Wang, T.; Wang, X.; Gu, C. Enhanced Electrochemical Properties of Al_2O_3-Coated LiV_3O_8 Cathode Materials for High-Power Lithium-Ion Batteries. *J. Power Sources* **2014**, *245*, 698−705.

(28) Song, H.; Liu, Y.; Zhang, C.; Liu, C.; Cao, G. Mo-doped LiV_3O_8 Nanorod-Assembled Nanosheets as a High Performance Cathode Material for Lithium Ion Batteries. *J. Mater. Chem. A* **2015**, *3*, 3547−3558.

(29) Liu, L.; Jiao, L.; Sun, J.; Zhang, Y.; Zhao; Yuan, H.; Wang, Y. Electrochemical Performance of $LiV_{3-x}Ni_xO_8$ Cathode Materials Synthesized by a Novel Low-Temperature Solid-State Method. *Electrochim. Acta* **2008**, *53*, 7321−7325.

(30) Zhao, M.; Jiao, L.; Yuan, H.; Feng, Y.; Zhang, M. Study on the Silicon Doped Lithium Trivanadate as Cathode Material for Rechargeable Lithium Batteries. *Solid State Ionics* **2007**, *178*, 387−391.

(31) Song, H.; Luo, M.; Wang, A. High Rate and Stable Li-Ion Insertion in Oxygen-Deficient LiV_3O_8 Nanosheets as a Cathode Material for Lithium-Ion Battery. *ACS Appl. Mater. Interfaces* **2017**, *9*, 2875−2882.

(32) Mo, R.; Du, Y.; Zhang, N.; Rooney, D.; Sun, K. In Situ Synthesis of LiV_3O_8 Nanorods on Graphene as High Rate-Performance Cathode Materials for Rechargeable Lithium Batteries. *Chem. Commun.* **2013**, *49*, 9143−9145.

(33) Ju, B.; Wang, X.; Wu, C.; Yang, X.; Shu, H.; Bai, Y.; Wen, W.; Yi, X. Electrochemical Performance of the Graphene/Y_2O_3/$LiMn_2O_4$ Hybrid as Cathode for Lithium-Ion Battery. *J. Alloys Compd.* **2014**, *584*, 454−460.

(34) Wu, F.; Wang, M.; Su, Y.; Chen, S. Surface Modification of $LiCo_{1/3}Ni_{1/3}Mn_{1/3}O_2$ with Y_2O_3 for Lithium-Ion Battery. *J. Power Sources* **2009**, *189*, 743−747.

(35) Liang, G.; Xu, J.; Xu, W.; Shen, X.; Zhang, H.; Yao, M. Effect of Filler-Polymer Interactions on the Crystalline Morphology of PEO-Based Solid Polymer Electrolytes by Y_2O_3 Nano-Fillers. *Polym. Compos.* **2011**, *32*, 511−518.

(36) Pan, A.; Liu, J.; Zhang, J.; Cao, G.; Xu, W.; Nie, Z.; Jie, X.; Choi, D. W.; Arey, B. W.; Wang, C.; Liang, S. Template Free Synthesis of LiV_3O_8 Nanorods as a Cathode Material for High-rate Secondary Lithium Batteries. *J. Mater. Chem.* **2011**, *21*, 1153−1161.

(37) Sakunthala, A.; Reddy, M. V.; Selvasekarapandian, S.; Chowdari, B. V. R.; Selvin, P. C. Preparation, Characterization, and Electrochemical Performance of Lithium Trivanadate Rods by a Surfactant-Assisted Polymer Precursor Method for Lithium Batteries. *J. Phys. Chem. C* **2010**, *114*, 8099−8107.

(38) Zhang, F.; Shi, Y.; Sun, X.; Zhao, D.; Stucky, G. D. Formation of Hollow Upconversion Rare-Earth Fluoride Nanospheres: Nanoscale Kirkendall Effect During Ion Exchange. *Chem. Mater.* **2009**, *21*, 5237−5243.

(39) Huang, X.; Xue, G.; Wang, C.; Zhao, N.; Sun, N.; Wei, W.; Sun, Y. Highly Stable Mesoporous NiO-Y_2O_3-Al_2O_3 Catalysts for CO_2 Reforming of Methane: Effect of Ni Embedding and Y_2O_3 Promotion. *Catal.: Sci. Technol.* **2016**, *6*, 449−459.

(40) Chen, Z.; Jiang, S.; Guo, R.; Xin, B.; Miao, D. Microstructure and Photoluminescent Properties of Y_2O_3:Eu^{3+} Phosphors Synthesised by Precipitation and Combustion Methods. *Mater. Technol.* **2014**, *29*, 198−203.

(41) Cai, Y.; Zhou, J.; Fang, G.; Cai, G.; Pan, A.; Liang, S. $Na_{0\cdot282}V_2O_5$: A High-Performance Cathode Material for Rechargeable Lithium Batteries and Sodium Batteries. *J. Power Sources* **2016**, *328*, 241−249.

(42) Mai, L.; Xu, X.; Han, C.; Luo, Y.; Xu, L.; Wu, Y.; Zhao, Y. Rational Synthesis of Silver Vanadium Oxides/Polyaniline Triaxial Nanowires with Enhanced Electrochemical Property. *Nano Lett.* **2011**, *11*, 4992−4996.

(43) Liu, Y.; Zhou, X.; Guo, Y. Structure and Electrochemical Performance of LiV_3O_8 Synthesized by Solid-State Routine with Quenching in Freezing Atmosphere. *Mater. Chem. Phys.* **2009**, *114*, 915−919.

(44) Xiong, X.; Wang, Z.; Guo, H.; Li, X.; Wu, F.; Yue, P. High Performance LiV_3O_8 Cathode Materials Prepared by Spray-Drying Method. *Electrochim. Acta* **2012**, *71*, 206−212.

(45) Yang, H.; Xu, G.; Wei, X.; Cao, J.; Yang, L.; Chu, P. Ultrafast Hetero-Assembly of Monolithic Interwoven V_2O_5 Nanobelts/Carbon Nanotubes Architectures for High-Energy Alkali-Ion Batteries. *J. Power Sources* **2018**, *395*, 295−304.

(46) Que, L.; Yu, F.; Wang, Z.; Gu, D. Pseudocapacitance of TiO_{2-x}/CNT Anodes for High-Performance Quasi-Solid-State Li-Ion and Na-Ion Capacitors. *Small* **2018**, *14*, No. 1704508.

(47) Ning, G.; Zhang, S.; Xiao, Z.; Wang, H.; Ma, X. Efficient Conducting Networks Constructed from Ultra-Low Concentration Carbon Nanotube Suspension for Li Ion Battery Cathodes. *Carbon* **2018**, *132*, 323−328.

(48) Chen, H.; Zhang, B.; Wang, X.; Dong, P.; Tong, H.; Zheng, J.; Yu, W.; Zhang, J. CNT-Decorated $Na_3V_2(PO_4)_3$ Microspheres as a High-Rate and Cycle-Stable Cathode Material for Sodium Ion Batteries. *ACS Appl. Mater. Interfaces* **2018**, *10*, 3590−3595.

(49) Li, L.; Xu, Y.; Sun, X.; He, S.; Li, L. High Capacity-Favorable Tap Density Cathode Material Based on Three Dimensional Carbonous Framework Supported $Na_3V_2(PO_4)_2F_3$ Nanoparticles. *Chem. Eng. J.* **2018**, *331*, 712−719.

(50) Jiang, T.; Wei, Y.; Pan, W.; Li, Z.; Ming, X.; Chen, G.; Wang, C. Preparation and Electrochemical Studies of $Li_3V_2(PO_4)_3$/Cu Composite Cathode Material for Lithium Ion Batteries. *J. Alloys Compd.* **2009**, *488*, L26−L29.

(51) Wang, L.; Wu, Z.; Zou, J.; Gao, P.; Niu, X.; Li, H.; Chen, L. Li-Free Cathode Materials for High Energy Density Lithium Batteries. *Joule* **2019**, *3*, 2086−2102.

(52) Wan, Z.; Lei, D.; Yang, W.; Liu, C.; Shi, K.; Hao, X.; Shen, L.; Lv, W.; Li, B.; Yang, Q.; Kang, F.; He, Y. All-Solid-State Batteries: Low Resistance-Integrated All-Solid-State Battery Achieved by $Li_7La_3Zr_2O_{12}$ Nanowire Upgrading Polyethylene Oxide (PEO) Composite Electrolyte and PEO Cathode Binder. *Adv. Funct. Mater.* **2019**, *29*, No. 1805301.

(53) Cho, S.; Kim, S.; Kim, W.; Kim, S.; Ahn, S. All-Solid-State Lithium Battery Working without an Additional Separator in a Polymeric Electrolyte. *Polymers* **2018**, *10*, No. 1364.

(54) Choudhury, S.; Stalin, S.; Deng, Y.; Archer, L. A. Soft Colloidal Glasses as Solid-State Electrolytes. *Chem. Mater.* **2018**, *30*, 5996−6004.

(55) Strauss, F.; de Biasi, L.; Kim, A. Y.; Hertle, J.; Schweidler, S.; Janek, J.; Hartmann, P.; Brezesinski, T. Rational Design of Quasi-Zero-Strain NCM Cathode Materials for Minimizing Volume Change Effects in All-Solid-State Batteries. *ACS Mater. Lett.* **2020**, *2*, 84−88.

(56) Wetjen, M.; Kim, G. T.; Joost, M.; Appetecchi, G. B.; Winter, M.; Passerini, S. Thermal and Electrochemical Properties of PEO-LiTFSI-Pyr(14) TFSI-Based Composite Cathodes, Incorporating 4 V-Class Cathode Active Materials. *J. Power Sources* **2014**, *246*, 846−857.

https://dx.doi.org/10.1021/acsami.0c18993
ACS Appl. Mater. Interfaces 2021, 13, 8219−8228